Michael C. Gibson

Department of Informatics and
Systems Engineering,
Cranfield University,
Defence Academy College of
Management and Technology,
Shrivenham, Wiltshire, SN6 8LA, UK
e-mail: m.c.gibson@cranfield.ac.uk

Amer Hameed

e-mail: a.hameed@cranfield.ac.uk

John G. Hetherington

e-mail: j.g.hetherington@cranfield.ac.uk

Department of Engineering
and Applied Science,
Cranfield University,
Defence Academy College of
Management and Technology,
Shrivenham, Wiltshire, SN6 8LA, UK

Investigation of Driving Force Variation During Swage Autofrettage, Using Finite Element Analysis

Swaging is one method of autofrettage, a means of prestressing high-pressure vessels to increase their fatigue lives and load bearing capacity. Swaging achieves the required deformation through physical interference between an oversized mandrel and the bore diameter of the tube, as it is pushed along and through the bore of the tube. A finite element (FE) model of the swaging process, developed previously by the author in ANSYS, was configured for comparison with an earlier model; this allowed the accuracy of further properties of the ANSYS model to be investigated. Driving force was the main property of interest, specifically how it varied with mandrel slopes and parallel midsection, to allow direct comparison with the earlier model. The variation of driving force with respect to coefficient of friction was investigated; driving force increased in near proportion, but a subtle trend indicated a further study of stress component be made. This was followed by a two-pass swage process. Close agreement was found with empirical data and the discrepancies observed between the two models are explained by the relatively coarse mesh used by the earlier model. This further verifies the sensitivity of the model described here.
[DOI: 10.1115/1.4006922]

Introduction

Swaging is used to introduce compressive residual stresses around cylindrical holes via the plastic expansion of the influenced region; such expansion is caused by the physical interference between the hole and an oversized mandrel that is forced through the hole (see Fig. 1). Earlier authors [1,2] have investigated the process for holes of small length to radius (l_z/r_a) ratios (eg holes through aluminium alloy fuselage panels), but holes of larger l_z/r_a ratios within steel tubes have not been the subject of openly reported investigations.

To address this, a finite element analysis (FEA) model of swage autofrettage was created by Gibson et al. [3] within the ANSYS FEA package, and then refined in a number of stages; here, it will be referred to as the ANSYS model. Initially, a like-for-like comparison was conducted with an early model developed by O'Hara [4], in the ABAQUS FEA package, which assessed a coarsely meshed single geometry of intermediate l_z/r_a. A sensitivity analysis was conducted to determine what characteristics were required to calculate meaningful midsection properties, and finally a parametric analysis was conducted. A summary of the findings and the modeling methodology developed are given below.

Iremonger and Kalsi's results [5] were used to investigate the accuracy of the mandrel driving force predicted by the ANSYS model (described in Ref. [3]). Driving force is a good measure of model fidelity as it depends on several properties: stresses developed, contact angles, and friction. As the model used in Ref. [5] was constructed in different analysis software, incorporating different numerical modeling methods, agreement between the two models would indicate mutual validation of modeling methodology. Additionally, Iremonger and Kalsi quote a value of driving force measured during an actual swaging run, to provide empirical validation.

The above allowed for a broad reaching assessment to be made of the ANSYS model, which established the preliminary work to allow further studies to investigate separate areas in greater depth.

General Modeling Notes

The basic geometry of the model used throughout these analyses (and by Iremonger and Kalsi [5]) is shown below in Fig. 1; it illustrates the pertinent tube dimensions and constraint, the travel of the mandrel and the location of the radial path at midaxial length ($l_z/2$) along which results are taken.

A cylindrical tube was used throughout these analyses; this matched that required for the initial comparison, and continued to be a sensible geometry on which to base the subsequent investigations. The rotational symmetry of both tube and mandrel about a common axis allowed the system to be defined as axisymmetric; this reduces the model down into a 2D section of half of the 3D system (allowing greater mesh fineness and/or more rapid solution).

The material is represented as a bilinear kinematic model (see Fig. 2), again, as required for this initial comparison; however, a more realistic, nonlinear, material model will be used in future analyses.
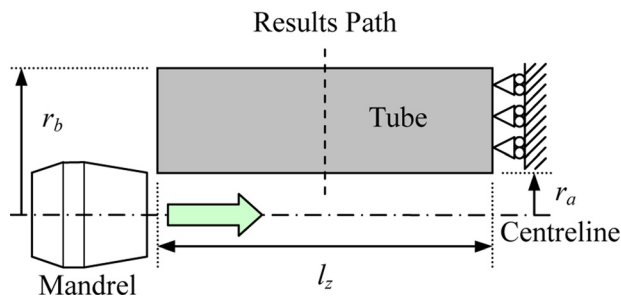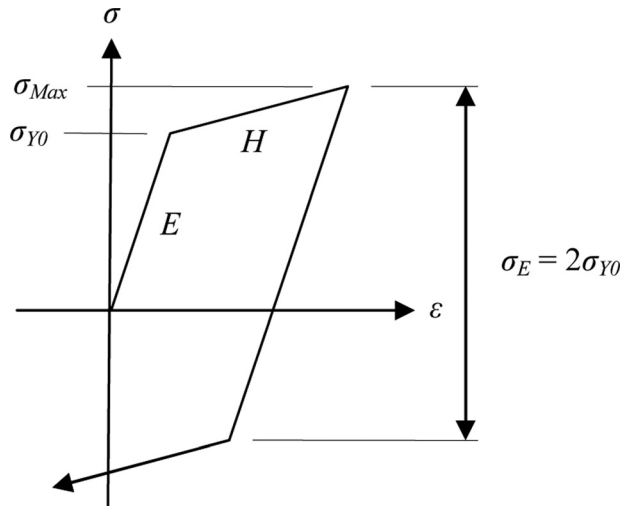

Fig. 1 System diagram

Fig. 2 Bilinear kinematic material model

This means the process is considered to be isothermal, which neglects the heating caused by stress–strain hysteresis and friction between the mandrel and tube. To model such characteristics would require information on the temperature dependent properties of the model, namely:

1. Softening of material due to temperature, altering reverse yielding
2. Nature of friction relationship

Phenomena such as the Bauschinger effect do have a strong influence on the development of the all important near-inner diameter (ID) compressive residual stresses during autofrettage. Due to the characteristic early onset of nonlinearity when unloading from prior plastic strain, reyielding in this region is exaggerated compared to that predicted by an elastic, perfectly plastic material.

It is unlikely either the Bauschinger effect or thermal softening would have a large influence on driving force, as each would alter tube material properties only toward the rear of the mandrel. Due to the plastic expansion of the tube, the area and pressure of contact on the rear slope of the mandrel are reduced compared to the front slope. Hence, these material properties have less importance in a driving force analysis than when predicting residual stresses.

Even were it not required for comparison a bilinear kinematic model would be acceptable for this investigation; it focuses upon the mechanisms that influence the prediction of mandrel driving force during swaging, rather than the response of a specific material under such conditions.

The geometry and dimensions (specifically the maximum radius, r_M, length of parallel section, l_{ll}, and forward and reverse slopes, θ_{MF} and θ_{MR}, respectively) of the swage are illustrated below, in Fig. 3.
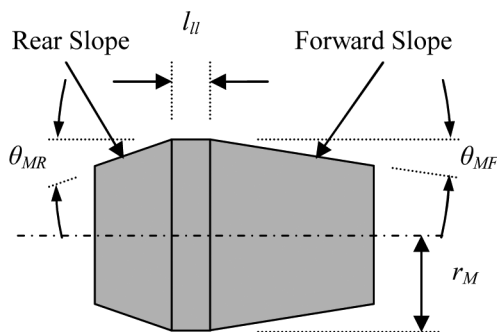
Swaging is a low velocity process, typically being conducted with a real-world mandrel velocity of 0.005 m/s. As such, both strain rate and inertial effects are small enough to be neglected in an analysis such that presented here.

Iremonger and Kalsi used PR2D, a 2D explicit Lagrangian code (i.e., a "hydrocode"), whereas the analysis presented here used ANSYS Mechanical APDL (ANSYS "Classic")—again a Langrangian-based code, but one that uses implicit time integration (i.e., traditional FEA—as used in Ref. [4]). While each code achieves solution in a quite different manner, they are both capable of solving a low strain rate, low velocity (inertia) scenario such as swaging.

The implicit code used here does not model velocity; it instead simulates the motion of the mandrel as a succession of steady-state analyses between which deformations are retained.

Explicit time integration does model velocity (and momentum) and requires solution to be achieved using a series of discrete intermediate solutions. The duration (in model time) between successive intermediate solutions must be less than a certain value (controlled by the Courant condition, which is determined by element size and speed of sound in the material) to maintain a stable solution and ensure propagation of events (e.g., stress waves). Hence, the number of intermediate solutions required to analyze a given system will depend on the duration of the event in question. For this reason, Iremonger and Kalsi utilized an elevated mandrel speed (reducing the number of intermediate solutions by a factor of ∼2000) to obtain a solution in a practical time.

In summary, both of the compared models represent the tube material has bilinear (i.e., no strain rate effects are present) and the increased inertial forces present in Iremonger and Kalsi's model would still be small in magnitude relative to the stresses due to deformation given the small distance moved radially (hence small velocity) by the tube. Hence, both models were considered to be equivalent and comparison is appropriate and meaningful.

Finite Element Model

The following notes on the generation of FE models are common throughout the different analyses presented here. Mesh geometry and sizing is defined as shown in Fig. 4. PLANE182 elements were used throughout; they are four-node linear elements, to which the axisymmetric property may be applied, and hence are suitable for the analysis.

Quadratic (eight-node) elements were used in the previous comparison [3]; however, it was found that four-node elements provided equally accurate results and solved more rapidly—in 1.517 rather than 2.882 h (as would be expected). Additionally, the ANSYS Contact Analysis Guide [6] recommends that elements with midside nodes should not be used during contact analyses.

Contact Pair Creation

The exact nature of the contact algorithm used in Ref. [5] is not explicitly stated, hence, the authors assumed the same contact
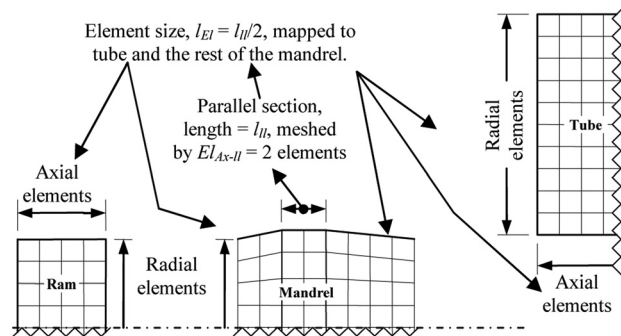

Fig. 3 Mandrel diagram

Fig. 4 Mesh sizing diagram

properties as used by O'Hara [4] as an initial state. The model used in the investigation described here used the same contact pair as in Ref. [4] hence no reasoning is presented here, only a summary of settings:

A flexible–flexible, symmetric contact pair was used, with frictional stresses defined by the Coulomb model (Eq. (1)), selecting isotropic variant (nondirection dependent).

$$\sigma_{rz} = \mu\sigma_r|_{r=ra} + \text{Cohesion} \qquad (1)$$

Friction coefficient was set to 0.015 as was the case during the comparison with O'Hara's results [4], (simulating a stearate-based high-pressure lubricant held at the contact surface in a porous phosphate coating) and cohesion to zero (in practice the interaction would be effectively cohesionless). Although Bihamta et al. [7] suggest a higher value of $0.05 \leq \mu \leq 0.18$, the value of 0.015 was retained to allow comparison with the earlier results [3]. For comparison, in the case of a lubricated sliding contact between two surfaces of hardened steel, μ can be taken as 0.05–0.15 [8].

A flexible–flexible contact denotes that both contacting bodies may deform, and a symmetric contact denotes that both bodies are of similar stiffness. While it was recognized that the mandrel would be stiffer than the tube, in terms of both material and geometry, it was felt that the deflection (which causes the plastic deformation required for autofrettage) of the tube was sufficiently important to ensure its accurate calculation by reducing penetration.

Accordingly, a symmetric contact was specified by applying TARGE169 and CONTA171 to both the tube inner diameter (ID) and mandrel surfaces. A comparison showed that a model using a symmetric contact pair required approximately 3% longer to solve than when an asymmetric contact pair was used; this was felt to be a suitable accuracy-performance trade-off.

Initial Comparison and Mesh Sensitivity

Iremonger and Kalsi [5] modeled the swage autofrettage of a relatively short length of steel tube, $l_z = 0.18041$ m, $r_a = 0.053975$ m, hence $l_z/r_a = 3.343$, of moderate wall ratio, $K = 2.103$. The mandrel's material is not stated but was considered to consist of tungsten carbide ($E_{\text{Swage}} = 500$ GPa, $\nu_{\text{Swage}} = 0.24$, $\sigma_{Y0\text{-Swage}} = 3390$ MPa, $H_{\text{Swage}} = E_{\text{Swage}}/10$) as was the case in Ref. [3]; its maximum radius, r_M, was set to 0.05541 m, hence, interference = 2.659% (with respect to the tube ID) along a parallel section of 0.0099 m ($0.183r_a$). The forward slope, θ_{MF}, equalled 3.0 deg, and the rear slope, θ_{MR}, equalled 1.5 deg. The tube is stated as having a static yield stress (σ_{Y0}) of 1068 MPa and behaving in an elastic, perfectly plastic manner (i.e., $H = 0$ Pa); Young's modulus and Poisson's ratio are not listed but are assumed to be standard values of 209 GPa and 0.3, respectively. These were entered into the presented model with the exception of tangent modulus as ANSYS requires $H > 0$ to avoid numerical singularities; accordingly, it was set to $E/10^{12}$ which is small enough to accurately approximate elastic, perfectly plastic behavior.

The interface between the swage and tube is not stated but is assumed to be a low friction sliding contact of the form of the Coulomb model. The finite element model was configured to match the above description.

The pertinent values regarding model configuration, determined by Ref. [3], are listed in Table 1.

Table 1   Model parameters

Property	Value
Axial elements, El_{Ax-ll}	4
Tube section length, l_z	$15r_a$
Time steps per element length (min, initial, max)	2, 10, 20
Friction coefficient, μ	0.015

The tube entry and exit slopes from the initial analyses are not modeled here. The initial diameters of the slopes are listed in Ref. [5] but not the length of taper, hence the decision to leave the rectangular section of the tube unmodified.

The sensitivity of the predicted mandrel driving force was the subject of the first comparison with the data from Ref. [5]. The parameters from Table 1 were used to configure the ANSYS FEA, while element size throughout the model was varied. Element size was varied based on the number of axial elements along the mandrel's parallel section (El_{Ax-ll}). The predicted driving forces, generated by this set of models, are compared with those from Ref. [5], labeled I-K, in Fig. 5.

The results in Fig. 5 demonstrate that driving force does depend on element size, but that once El_{Ax-ll} equals four or more the variation becomes minimal.

The results from Ref. [5] are consistently higher than those predicted by the model presented here; as the coefficient of friction used in Ref. [5] is not known this would seem to suggest they used a higher value of μ. However, Iremonger and Kalsi also note that driving force was empirically measured as "about 100T." In addition, they felt that their predicted value of driving force would decrease if the mesh were refined.

The mean values of driving force recorded from the presented model, over the 15–85% range of mandrel distance travelled, are listed in Table 2; they have been converted from Newtons to tonnes to simplify comparison with the stated empirical value. Errors are relative to results from the next, more refined mesh.

The decreasing relative error indicates the model is stable and responds as would be expected to reductions in element size. The absolute values of the driving forces predicted also indicate the model reflects the real-world conditions during the swaging process reported in Ref. [5].

The results from Ref. [5] also increase and peak more rapidly than those presented here. This is most likely due to the absence of taper angles at the entrance of the tube in the ANSYS model, in addition to the lower force predicted by the ANSYS model. However, given the absence of slope angles it is still felt the omission of tapers was justified.

Tube Length Sensitivity

The influence of tube length was then investigated, to determine whether the $l_z = 15r_a$ condition selected in Ref. [3] also held true when predicting driving forces. Model parameters were as listed in Table 1, with the exception that l_z was varied from $5r_a$ to $40r_a$, in steps of $5r_a$. The resultant driving forces are plotted against mandrel distance travelled in Fig. 6.

The observed driving forces exhibit a consistent midrange value once $l_z \geq 10r_a$, indicating that $l_z = 15r_a$ is a suitable choice for the investigation of midtube phenomena while remaining computationally feasible. This agrees with similar observations of residual axial stresses following swaging in Ref. [9].

Mandrel Geometry Variation

Having conducted an initial check of model sensitivity to element size and tube section length, a series of three independent variations were made to the base configuration which each then underwent a swaging procedure. The variations matched those made in Ref. [5] and are as follows:

1. Entry slope, θ_{MF}, of the swage increased to 6 deg.
2. Exit slope, θ_{MR}, at the rear of the swage increased to 4.5 deg.
3. Parallel section length (l_{ll}) over which the swage has a maximum (uniform) diameter was reduced to 6.6 mm.

The driving force data from the three variants described above are plotted against mandrel distance travelled, in Figs. 7–9, respectively.
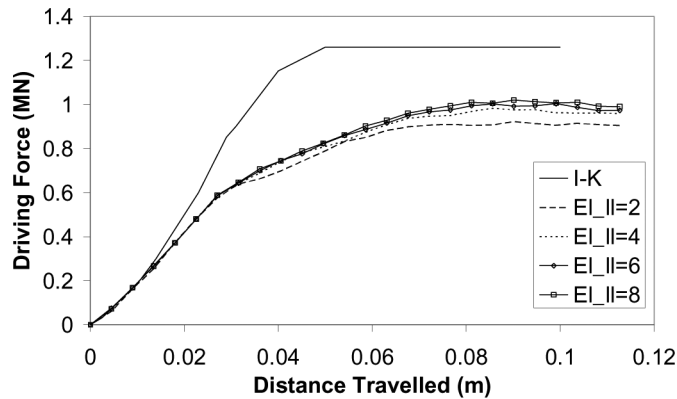
Fig. 5   Initial driving force comparison

Table 2   Driving force values, element size variation

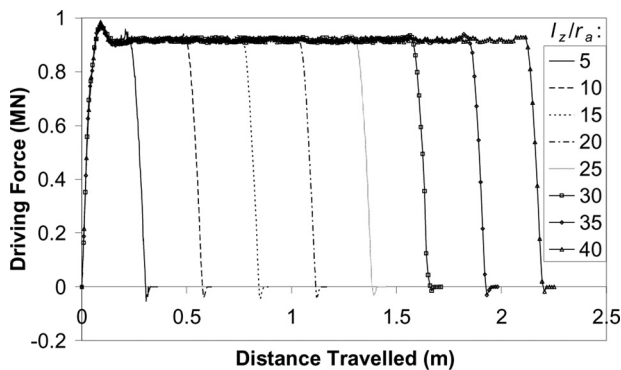| El$_{Ax-ll}$	Value (T)	% relative error
2	87.42	−6.864
4	93.86	−2.437
6	96.21	−1.667
8	97.84	n/a

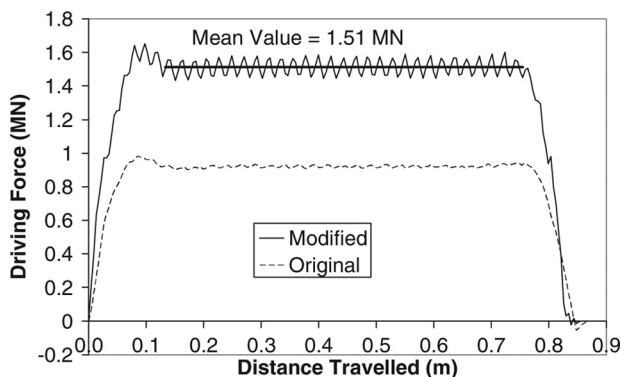

Fig. 6   Driving force versus tube length comparison

Fig. 7   Driving force for θ_{MF} = 6 deg

As shown by Fig. 7, increasing the front taper (θ_{MF}) of the mandrel from 3 deg to 6 deg increased the mean midtube driving force by more than 50% (from an initial value of 0.921 MN), whereas changes to the rear taper (θ_{MR}) and parallel section length (l_{ll}) had relatively little effect (Figs. 8 and 9, respectively).

Resistance to the motion of the mandrel arises primarily from friction and the axial component of contact pressures acting on
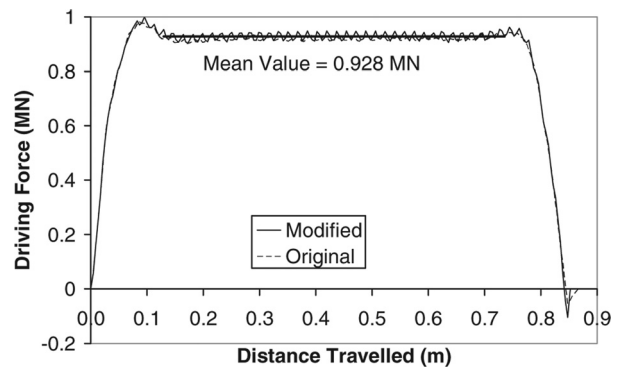

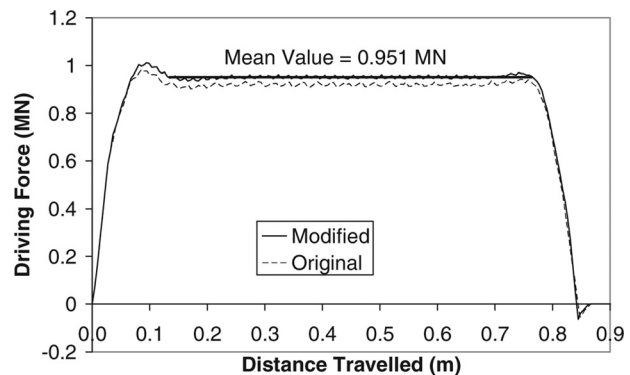Fig. 8   Driving force for θ_{MR} = 4.5 deg

Fig. 9   Driving force for l_{ll} = 6.6 mm

the tapered sections. The large increase in mean driving force observed when θ_{MF} is doubled (first variant) indicates that the axial component of contact stresses dominates the reduced frictional force that results from the reduced contacting area due the steeper angle. This is expected for low values of μ. This indicates that the rate of change of radial deflection with respect to axial position has a strong effect on contact pressure. This corresponds with large shear stresses developed near the ID that were observed in Ref. [3] when mandrel slopes were increased. Taking the above points together suggests large radial stresses are developed in conjunction with large shear stresses; this interplay of stress components will be investigated in more detail in a future publication.

The far more modest increase in driving force observed (Fig. 8) when the rear taper angle is increased indicates that the contact pressure is much reduced over that encountered at the front taper and hence its axial component makes little effect on the overall

	Table 3	Mean driving force variation		
	ANSYS model		I-K model	
Case	Value (MN)	% relative change	Value (MN)	% relative change
1	1.511	64.14	1.520	23.02
2	0.928	0.7743	1.000	−19.05
3	0.951	3.306	1.148	−7.143

	Table 4	Mean driving force variation
μ	Value (MN)	Increase (MN)
0.000	0.599	n/a
0.015	0.915	0.316
0.030	1.232	0.317
0.045	1.550	0.318
0.060	1.869	0.320
0.075	2.189	0.319
0.090	2.514	0.326

resistance to motion. This is expected, given the plastic expansion of the tube (the modus operandi of swaging).

The above observations, on the results from the three variants, highlight the complex interplay between stress components during swaging. If the inclined areas of the mandrel (contact pressures acting on the area of the front and rear slopes create axial forces) are each taken to be the annular area, A_O, that overlaps with the tube

$$A_O = \pi \left(r_M^2 - r_a^2 \right) \qquad (2)$$

If this area remains constant for the front and rear slopes (the contacting area on the rear slope will be slightly lower, due to the permanent expansion of the tube), considerable variation in contact pressures must have developed when the front taper angle was increased.

Similarly, the decrease in parallel section length (l_{ll}) resulted in a very small change in driving force. A prima facie assessment of the shorter mandrel would suggest a lower frictional force due to its reduced area, but it would seem that the effect of the shorter section length on pressure distribution outweighs any area-based force reduction. This warrants a more thorough investigation of contact pressure over the mandrel surface, and shear stress development.

Coefficient of Friction Variation

Having conducted the above investigations, it was then logical to examine the effect of varying μ. A series of seven analyses were then carried out, specified in Table 1 as μ was varied from 0% to 9% in steps of 1.5%. The driving force-distance data are plotted in Fig. 10.

The plots in Fig. 10 exhibit what appears to be a constant difference between the midrange driving force values, suggesting a relationship of the following form between driving force and μ for the cohesionless Coulomb friction model used here:

$$F_D = F_{\mu=0} + k\mu \qquad (3)$$

The mean values are listed in Table 4 for greater precision; $F_{\mu=0}$ is given by the driving force in the $\mu = 0$ case. This results
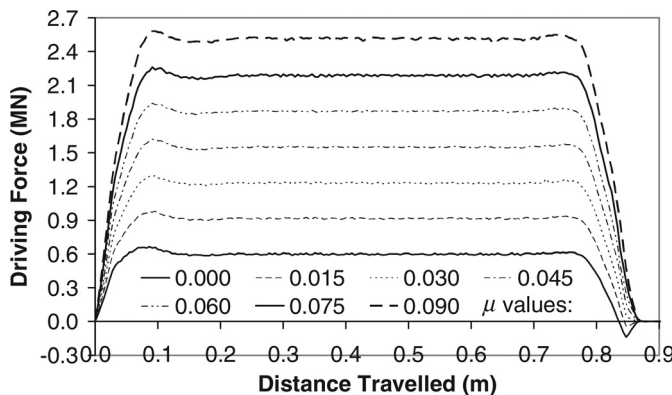
from a mean net pressure difference (which could be considered to act on the area A_O from Eq. (2)) between the front and rear slopes of the mandrel.

A small but seemingly consistent increase is observed in the difference between successive runs, which is thought to be due to variations in the stress distribution within the tube. This would change the shear stress distribution and hence the relationship between direct stress components and equivalent stress. This would be potentially significant in a postyield elastic, perfectly plastic material where equivalent stress remains constant; for example σ_r would almost certainly change. The relationship between μ, shear stress distribution and driving force will be the subject of a future publication.
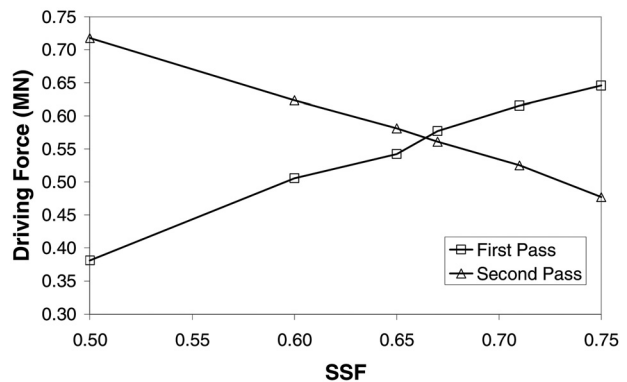
Two-Pass Swaging

The final investigation conducted in Ref. [5] was of two-pass swaging, in which the swaging of the tube using the mandrel described above was preceded by an initial pass was made by a similar subscale mandrel. The intention of the analysis was to size the subscale mandrel such that the driving force required for both passes matched at a lower value than that calculated for the single pass procedure initially modeled, to optimize the manufacturing process.

A series of two-pass swage configurations were simulated in the ANSYS model, in which the interference of the first mandrel was scaled as a proportion of the second mandrel, using the swage scaling factor, SSF. The second mandrel retained the same configuration as in the initial comparison (interference of 2.659%) and was used to swage the tubes once the first swage had passed fully through the tube.

The resulting driving forces for each swage (first and second pass) are plotted in Fig. 11 for SSF values of 0.50, 0.67, 0.71, and 0.75. Driving forces are calculated as the mean value taken over the 20–80% range of mandrel movement. This slightly narrower range was required to ensure consistent midrange values were used.

The ANSYS model predicted that an SSF value of 0.665 would result in equal driving forces for the first and second swage passes, of 0.567 MN. This compares quite closely with the interference

Fig. 10 Driving force versus μ Comparison

Fig. 11 Comparison of two-pass swage driving forces
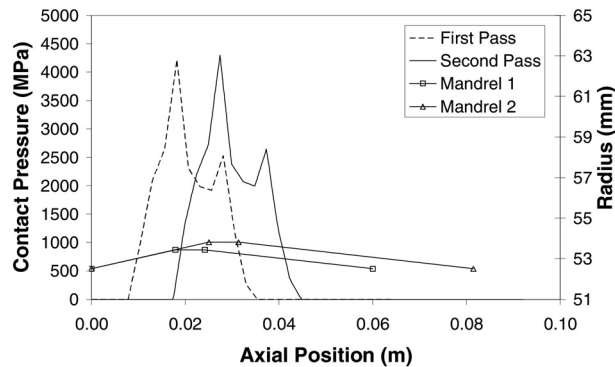
Fig. 12 Contact pressures over Mandrel surfaces during two-pass swaging (distances from front of mandrel)

ratio of 0.69 which resulted in a driving force of approximately 0.74 × the original value (i.e., 0.932 MN) found in Ref. [5]. The two-pass swage model was rerun with an SSF value of 0.665, which yielded driving forces for the first and second passes of 0.5658 MN and 0.5661 MN, respectively. At the mid tube length position, contact pressure profiles of the surface the mandrel were recorded for SSF = 0.665 and are plotted in Fig. 12.

While the values of driving force calculated by each model are different, the ratios between the driving forces calculated for the 1-pass and 2-pass cases are similar. In addition both models predict that first pass and second pass driving forces will become equal at an SSF of approximately 0.7. The prediction of similar SSF values also implicitly suggests that each model considers similar ratios of plastic deformation between the first and second passes. Taking together the above indicates the two different models provide mutual validation of each other, especially if a more refined mesh were used within PR2D.

However, the driving force for the second pass would vary were a more realistic material model incorporated into a model of swage autofrettage. This is also true of the pressure distribution over the mandrel surface. Many materials that autofrettaged tubes are fabricated from exhibit the Bauschinger effect, which describes the early onset of nonlinearity when unloading from prior plastic strain (as compared to the elastic, perfectly plastic model, for example).

As mentioned above, in general modeling notes, the Bauschinger effect may have some small effect on the driving force required for the first pass (or indeed, a one-pass swaging procedure), this effect would be minor, especially given the small influence of rear mandrel slope (see Fig. 8).

The Bauschinger effect would have a moderate effect on the driving force required by the second pass (or potentially, further passes), as the tube would undergo further reyielding following the first pass. The mandrel during the second pass would then be required to do more work during its passage through the tube.

While this is not an issue for the ANSYS model described here, the sensitivity of second pass driving force to the Bauschinger effect exhibited by the tube material would be a meaningful test of the fidelity of a future swage autofrettage model that incorporated realistic material behavior. The effect of the Bauschinger effect on first pass driving force may also be detectable, but is expected to be smaller in magnitude.

However, it must be confirmed that residual stress distributions resulting from two-pass swaging are comparable with those resulting from one-pass swaging and achieve suitable prestressing of the tube. This will be the subject of a future investigation.

Summary of Discussions

Inspection of the solution monitoring output from ANSYS revealed consistent progression of solution; equilibrium iterations per substep were fairly constant during a given solution, and increased in near-linear correlation with El_{Ax-ll}.

The results indicate that prediction of stable mandrel driving forces is more sensitive to element size than calculations of smooth stress contours are. The fluctuations, as seen in Fig. 7 for example, are caused by a combination of the making and breaking of contact between individual elements as the mandrel travels along the length of the tube (this is also mentioned in Ref. [5]) and the sampling frequency of results. Although these could be lessened by the use of smaller elements and more frequent sampling, a more elegant solution may be the use of a different contact algorithm and/or different contact algorithm settings.

The mean values of driving force, given in Table 2, do appear to reduce in terms of relative error at a similar rate to values of stress used to gauge accuracy in Ref. [3].

The exact nature of the friction between the mandrel tube in the empirical test quoted in Ref. [5] is not stated, but the assumed model and friction coefficient (this was investigated and $\mu = 0.015$ was the closest match to the quoted force by a large margin—see Fig. 10) appear to match the force quite closely.

However, setting $El_{Ax-ll} = 4$ still seems to be an optimum value given the simple friction and material models used; they could each cause several percent error. Each will be the subject of future study to enable refinement of the ANSYS model, after which it would be appropriate to reassess its accuracy-computational cost balance.

The front slope of the mandrel had a far greater effect on the required driving force due to the rate of change of radial deflection that results. Due to the plastic expansion of the tube, its negative deflection as it contracts along the rear slope of the mandrel is smaller (hence rate of change of axial deflection is less). A detailed study of the relationship between slope, relative mix of stress components and required driving force will follow.

During hydraulic autofrettage, loading is considered uniform along the tube's length, hence radial expansion is uniform and surfaces initially parallel to the axis remain so. This means that radial stresses are the sole means of distributing radial force through the tube wall. The localized nature of loading that occurs during swaging causes uneven deflection of the tube; surfaces initially parallel to the axis do not remain so. Radial, axial and shear stresses then all become factors in the distribution of the radial force through the tube wall.

When mandrel slopes were increased in Ref. [3], in the near inner diameter (ID) region large shear stresses were observed during swaging and large negative (compressive) residual axial stresses were developed (Figs. 16 and 18 in Ref. [3], or may also be found in Ref. [9]). This highlights how the axial variation of radial deflection is the key factor in swage autofrettage, due to its effect on plastic axial strains developed during the process.

The two-pass swaging comparison yielded different values of the optimized driving force, although the similar ratios found between the results of each model suggest that both predict similar ratios of plastic deformation between passes. It is expected that driving force for the second pass will be sensitive to the degree of Bauschinger effect displayed by the tube material when unloading.

Conclusion

A close match is observed between the driving force predicted by the ANSYS model and the empirical value quoted in Ref. [5], with caveats regarding the precise nature of mandrel-tube friction and tube stress–strain behavior when unloading from prior plastic strain. However, as discussed, it is felt that each uncertainty would be of small magnitude; hence, the close match indicates the ANSYS model is a useful predictor of mandrel driving force required during swaging. Greater confidence would be gained from further comparisons with empirical data.

Both models predicted that variation in the front slope of the mandrel would have a large effect on the required driving force,

while the rear slope and parallel section length would have comparatively smaller effects.

The required driving force predicted by the ANSYS model rose consistently and in near proportion to the coefficient of friction, although there is some evidence of relative change between the values of the stress components present.

The ratio of driving forces in the optimized 2-pass and 1-pass cases is reassuring, although driving forces predicted for the second pass are most sensitive to material behavior (particularly when unloading from prior plastic strain) and hence, these values should be treated with less confidence. However, the model does demonstrate the ability to reduce the required mandrel driving force via two-pass swaging; this will be further investigated, as well as the effect of multipass swaging on residual stress development.

Taken with the findings in Ref. [3] provide further validation of the ANSYS model.

Nomenclature

A_O = Annular area of mandrel slopes, viewed along its axis
E = Loading and unloading Young's modulus
El_{Ax} = Number of axial elements in mesh of tube
$El_{Ax\text{-}ll}$ = Number of axial elements along the parallel section of mandrel
$El_{N\text{-}Ax}$ = Number of axial element lengths, l_{El}, moved by the mandrel as it passes through the tube undergoing swage autofrettage (a distance of $l_z + l_m$)
F_D = Mandrel driving force
$F_{\mu=0}$ = Zero friction mandrel driving force
H = Tangent modulus
k = Constant of proportionality relating μ and frictional component of mandrel driving force
K = Tube wall ratio, r_b/r_a
l_{ll} = Length of parallel section of mandrel
l_z = Tube section length
r_a, r_b = Inner and outer tube radii
r_M = Mandrel radius (to parallel portion)
SSF = swage scaling factor (interference of first pass mandrel/ interference of second pass mandrel)
θ_{MF} = Angle between axis and forward taper of mandrel
θ_{MR} = Angle between axis and rear taper of mandrel
μ = Coefficient of friction
σ_E = Elastic stress range between peak plastic strain and onset of reverse yielding
σ_{Max} = Maximum stress reached during initial deformation
σ_r = Radial stress
σ_{rz} = Shear stress, acting on the plane normal to the radial direction, in the axial direction
σ_{Y0} = Initial yield stress, in simple tension

References

[1] de Matos, P. F. P., Moreira, P. M. G. P., Camanho, P. P., and de Castro, P. M. S. T., 2005, "Numerical Simulation of Cold Working of Rivet Holes," Finite Elements in Analysis and Design, **41**(9–10), pp. 989–1007.

[2] de Matos, P. F. P., Moreira, P. M. G. P., Pina, J., Dias, A. M., and de Castro, P. M. S. T., 2004, "Residual Stresses Around an Expanded Hole in an Aluminum Clad Sheet," Proceedings of the 7th International Conference on Residual Stress (ICRS7), CD ROM, Xi'an, China, June 14–16.

[3] Gibson, M. C., Hameed, A., and Hetherington, J. G., 2009, "Investigation of Residual Stress Development During Swage Autofrettage, Using Finite Element Analysis," Proceedings of the ASME 2009 International Mechanical Engineering Congress and Exposition (IMECE2009), Nov. 13–19, Lake Buena Vista, Florida, Paper No. IMECE2009-13289.

[4] O'Hara, G. P., 1992, "Analysis of the Swage Autofrettage Process," Benét Laboratories, Watervliet Arsenal, NY, US Army ARDEC Technical Report No. ARCCB-TR-92016.

[5] Iremonger, M. J. I., and Kalsi, G. S., 2003, "A Numerical Study of Swage Autofrettage," J. Pressure Vessel Technol., **125**(3), pp. 347–351.

[6] ANSYS Contact Technology Guide, ANSYS Release 11.0 Documentation, ANSYS, Inc.

[7] Bihamta, R., Movahhedy, M. R., and Mashreghi, A. R., 2007, "A Numerical Study of Swage Autofrettage of Thick-Walled Tubes," Mater. Des., **28**, pp. 804–815.

[8] 1974, Tribology article, *Encyclopædia Britannica*, Vol. 11.

[9] Gibson, M. C., 2008, "Determination of Residual Stress Distributions in Autofrettaged Thick-Walled Cylinders," Doctoral Thesis, Cranfield University, Shrivenham, United Kingdom.